



NIH Public Access

Author Manuscript

Langmuir. Author manuscript; available in PMC 2010 May 18.

Published in final edited form as:

Langmuir. 2007 October 9; 23(21): 10672–10681. doi:10.1021/la070214v.

Computational Modeling of Poly(alkylthiophene) Conductive Polymer Insertion into Phospholipid Bilayers

Alik S. Widge[†], Yoky Matsuoka[‡], and Maria Kurnikova^{*}

Carnegie Mellon University, Pittsburgh, Pennsylvania 15213

Abstract

We have previously demonstrated that some poly(alkylthiophenes) (PATs) are able to increase the electrical conductance of unsupported phospholipid bilayers and have hypothesized that this effect is due to the ability of some PAT side chains to permit stable insertion into the bilayer. We have further proposed the development of long-term intracellular electrodes based on that phenomenon. In this article, we apply molecular dynamics techniques to study the insertion of two model PATs into a patch of a lipid bilayer. Steered molecular dynamics is used to obtain potential trajectories of insertion, followed by umbrella sampling to determine the free-energy change upon insertion. Our results indicate that both branched-side-chain poly(3-(2-ethylhexyl)thiophene) (EHPT) and straight-side-chain poly(3-hexylthiophene) (HPT) are able to enter the bilayer but only EHPT can cross the center of the membrane and establish an electrical bridge. HPT penetrates the head groups but is not able to enter the alkyl tail phase. These findings support the feasibility of our electrode concept and raise questions regarding the mechanisms by which branched side chains grant PATs greater solubility in a lipid bilayer environment. The parameters and methods used in this study establish a novel framework for studying these and similar systems, and the results hold promise for the use of EHPT in biosensing and neural interfacing.

Introduction

Conductive polymers from the polythiophene family have in recent years attracted interest as possible biosensors because of their high conductivity, postsynthesis processability, and versatile array of end and side-chain functional groups.^{1,2} We have recently shown that an end-thiolated poly(alkylthiophene) (PAT) can form mixed self-assembled monolayers (SAMs) with alkanethiols and that such SAMs are biocompatible with primary mouse neurons.³ PATs organized in such a SAM could potentially be used for long-term intracellular recording and stimulation of living cells both *in vivo* and *in vitro* by inserting PAT “molecular wires” through the cell membrane in the fashion of ion channels. This concept is diagrammed in Figure 1. In experiments with unsupported bilayer lipid membranes (BLMs), we found that poly(3-(2-ethylhexyl)thiophene) (EHPT) is able to increase the electrical conductance of a BLM but poly(3-hexylthiophene) (HPT) is not.⁴ We have previously attributed this to the differential solubility of the two molecules, which is derived from the structure of their side chains (illustrated in Figure 2). EHPT’s branched side chain gives it greater solubility in saturated hydrocarbons, which should make it able to insert into a bilayer that HPT cannot enter. However, we have not yet been able to conclusively visualize or otherwise demonstrate the insertion mechanism of Figure 1, even though we believe it to be the most likely explanation for our observations.

*Corresponding author. kurnikova@cmu.edu.

[†]Present address: University of Pittsburgh School of Medicine, Pittsburgh, Pennsylvania 15261.

[‡]Present address: University of Washington, Seattle, Washington 98195.

Molecular dynamics simulations have been successfully used to model the insertion of a wide variety of hydrophobic molecules into lipid membranes. A representative sample of molecules includes mellitin (a pore-forming peptide toxin found in bee venom),^{5,6} antimicrobial peptides,⁷ 7 helical voltage sensors from voltage-sensitive potassium channels,⁸ the WALP model hydrophobic peptide,⁹ a monotopic protein,¹⁰ and large-channel proteins (using a “coarse-grained” model).^{11,12} Other closely related applications include an estimation of the energy of halothane partitioning from water into lipid¹³ and modeling the unfolding of a transmembrane peptide during AFM extraction.¹⁴

The polythiophenes have also proven amenable to computational chemistry treatments. A large fraction of recent work in this area is devoted to ab initio or density functional theory studies of the electron structure and emission/absorption properties of various polymers.² Molecular dynamics methods have been used to investigate the PAT conformation in different solvation regimes,^{15–17} the structure and pressure/temperature responses of doped and undoped solid-state PAT films,^{18,19} ion migration during PAT film doping,²⁰ and the orientation and dipole of an amphiphilic PT monolayer at an air/water interface.^{21,22}

In this article, we combine the above lines of investigation to model the insertion of single chains of EHPT and HPT into a patch of membrane. On the basis of prior BLM results and our proposed explanation, we initially hypothesize that EHPT has a favorable free energy of insertion whereas HPT’s is less favorable. We also expect the two polymers to follow different trajectories when insertion is forced through external constraints, with EHPT following a path that is more consistent with those of known transmembrane molecules. We begin by using steered molecular dynamics (SMD) to determine trajectories and then perform umbrella sampling at points along the trajectories to elucidate the potential of mean force. Through the results of these two sets of simulations, we will show that both model PATs initially appear to have negative free energies of insertion, which is discordant with our initial hypothesis. However, they do show the predicted difference in trajectory, and HPT’s final configuration is not truly inserted into the membrane. By examining these different configurations, we are able to better explain the results of our prior BLM studies and strengthen the proof of concept for a “molecular wire” transmembrane electrode.

Experimental Methods

Simulation Parameters and Coordinates

All simulations reported in this article used a system of a PAT decamer (either HPT or EHPT) interacting with a bilayer patch of 128 dimyristoylphosphatidylcholine (DMPC) phospholipids. DMPC was chosen as the model lipid because of its known gel-to-liquid transition temperature of 296 K; the other commonly used model, dipalmitoylphosphatidylcholine (DPPC), has a transition temperature above 310 K and would be in a gel phase during the simulations. Both the PATs and the lipids used a united-atom model in which aliphatic hydrogens were merged with their attached carbons. A similar model has recently been used to study the interaction of poly(ethylene oxide) with a DMPC bilayer.²³ Initial well-equilibrated coordinates for the bilayer and GROMACS²⁴ format united-atom parameters were obtained from Dr. D. Peter Tieleman.²⁵ To maintain consistency with the AMBER²⁶ format PAT parameters, the GROMACS lipid parameters were then translated by hand into an AMBER force field format, and their partial charges were replaced with previously known RESP-style charges.²⁷ In preliminary lipid-only simulations (not shown here) using an NPT ensemble, we found that these charges gave an area per lipid that was closer to the experimental value than did the GROMACS format charges (61.5 vs 64 Å²). AMBER format parameters and starting geometries for PATs were derived by ab initio calculation of the PAT inter-ring torsion energy and implicit solvent replica exchange simulation of the decamer chains; the details of this derivation are reported elsewhere.^{28,29} The combined system was

then constructed by placing either an EHPT or HPT decamer near one leaflet of the bilayer. The long axis of the polymer chain was placed parallel to the bilayer normal, and at least 12 Å of separation was maintained between any atom of the PAT and any atom of the bilayer. These coordinate manipulations and visualization of all simulation results were performed using the VMD program.³⁰

The initial PAT/DMPC system was solvated with TIP3P waters (6590 for EHPT/DMPC, 6610 for HPT/DMPC) and energy minimized, with the polymer backbone and the central glycerol atom of each DPMC molecule restrained in place. After minimization, the system was reheated to a temperature of 310 K and equilibrated over 100 ps. All simulations reported in this article used a constant volume/constant temperature (*NVT*) ensemble. The temperature was maintained at 310 K in all simulations, except for the SMD runs, using a Langevin thermostat with a time constant of 0.5 ps⁻¹. The simulation box was fixed to a size of 62 × 62 × 89 Å³, which corresponds to the empirically known area-per-lipid value of 60 Å² for DMPC.³¹ Although this constant-volume system may impose a surface tension on the bilayer, we felt that it was important to ensure the correct area per lipid. Other investigators have found that correcting this single parameter leads to overall good agreement between simulated and experimental bilayer structure using a variety of different measurements.³² Electrostatic interactions were handled using the particle mesh Ewald (PME) method, with the direct sum and VDW interactions truncated at 12 Å. All bonds involving hydrogen were constrained with the SHAKE algorithm, allowing an integration time step of 2 fs. The program NAMD (version 2.6b) was used for all simulations.³³ NAMD supports the AMBER force field format and most calculation options and has been optimized for efficient performance on highly parallel systems.

Steered Molecular Dynamics

Hypothetical trajectories for EHPT and HPT insertion into the DMPC bilayer (as well as very rough estimates of the energy of insertion) were obtained by SMD. The center of mass of the rings of the PAT decamer was pulled from a Z-axis distance of 52.5 Å away from the membrane center (an aqueous configuration parallel to the bilayer normal with the “N-terminal” ring 12 Å away from the membrane head groups) to 0 Å from the bilayer center (fully inserted). Because one long simulation is believed to be informationally equivalent to or better than several short simulations,^{34,35} the longest simulation feasible within the available computational resources was performed. The PAT decamers were pulled into the bilayer at a rate of 0.01 Å/ps with a force constant of 10 kcal/mol/Å. This was expected to be slow enough to capture the reaction pathway accurately on the basis of others’ observations of peptides in a translocon.³⁶ The initial configuration was heated as described above, but no temperature control was used during the SMD pull; experienced investigators have indicated that thermostats and barostats may distort free-energy calculations by adding and removing energy from the system.^{34,37} To improve the estimated accuracy further, the reverse reaction was also simulated by pulling EHPT and HPT decamers from the bilayer center to a point 52.5 Å along the Z axis from the center. Following the method of Kosztin et al.,³⁸ this should allow the removal of the frictional work component by averaging the forward and reverse energies. The initial configuration for the reverse pull was generated by superimposing the PAT and bilayer centers of mass and then minimizing and running dynamics for at least 1 ns with the polymer restrained to remain 0 Å away from the center. All SMD runs were set to output the applied force every 20 fs and to save the system coordinates every 1 ps. All four SMD runs taken together (21 ns of simulation time) required approximately 3500 processor hours on the Cray XT3 machine at the Pittsburgh Supercomputing Center.

Umbrella Sampling

As described below, the SMD pulls provided a good view of the reaction pathway for EHPT and HPT insertion but did not produce a reliable estimate of the free energy. This could be alleviated by pulling at a slower speed that approaches the fully reversible regime, but the optimal speed is estimated to be about $0.0001 \text{ \AA}/\text{ps}$.³⁹ Such a simulation would require more than 500 ns of total simulation time. Given the availability of a reaction path from the forward SMD runs, it is possible to apply umbrella sampling techniques to extract the PMF without multiple SMD pulls.

The reaction paths obtained from the forward SMD pulls of EHPT and HPT were used to seed a set of umbrella sampling simulations. A set of distances along the Z axis between the polymer center and bilayer center were selected, with these umbrella centers being spaced more closely within the bilayer and more sparsely in the aqueous phase (as a result of greater viscosity in the bilayer). Umbrella centers ranged from 1 Å below the bilayer center (a coordinate of -1 \AA) to 45 Å above the bilayer center ($+45 \text{ \AA}$). A harmonic restraining potential was applied to the Z coordinate of the center of mass of the PAT decamer, keeping it near the umbrella center. The SMD trajectory frame closest to the specified Z distance was chosen as the starting point for each window. These frames were re-equilibrated for 50 ps (with the harmonic umbrella potential in place) to relax the distortion caused by the SMD pull and were then run for 3 ns each to collect data. Additional windows were added as necessary to ensure sufficient overlap between histograms. The EHPT and HPT systems each required 28 windows for a total of 168 ns of simulation time. For EHPT, 21 windows used a force constant of $0.6162 \text{ kcal/mol}/\text{\AA}$ ($1k_B T$ at 310 K), and 7 used a force constant of $3 \text{ kcal/mol}/\text{\AA}$. For HPT, 9 windows used a force constant of $0.6162 \text{ kcal/mol}/\text{\AA}$, and 19 used $3 \text{ kcal/mol}/\text{\AA}$. After simulation, the processed trajectories and energies were combined using the WHAM method and the code of Chodera et al.,⁴⁰ which was properly modified to handle umbrella potentials using the direct-sum-over-data method of Kumar et al.⁴¹ Uncertainties in the PMF were estimated per the Chodera et al. procedure,³⁷ with all statistical inefficiency terms g^{-1} set to 1.

Results

SMD Reaction Path and Initial Energy Estimates

The forward and reverse SMD pulls reveal a likely reaction path for the insertion of EHPT or HPT into a DMPC bilayer. Root-meansquare (rms) errors between the commanded and actual polymer-to-bilayer distance (as measured using centers of mass) were 0.33 and 0.42 Å for the EHPT and HPT forward pulls, respectively. Both forward pulls showed the polymer rotating and reorienting itself as it inserted itself into the bilayer, suggesting that the pull rate of $0.01 \text{ \AA}/\text{ps}$ allowed the system to relax at least partially. The results for the reverse pull are less clear. The rms command-to-actual errors for the reverse pulls were 0.81 and 0.71 Å for EHPT and HPT, respectively. These errors are twice those of the forward pulls and suggest that the pull may have been too fast (or the spring constant too weak) to capture a reasonable trajectory for the removal reaction.

Before turning to the details of that path, it is useful to consider the differences in work done along the EHPT and HPT trajectories. The work done during forward and reverse pulls for both polymers is shown in Figure 3. By averaging the forward and reverse curves at each point along the trajectory and translating the resulting sum so that the origin (52.5 Å from the bilayer center) corresponds to zero energy, irreversible frictional work can in theory be discounted and the true PMF of insertion revealed.³⁸ The results of this averaging are also shown in Figure 3. As would be expected for an SMD run at this speed, both forward curves still contain substantial frictional work and have a positive energy of insertion. There is an inflection point in both forward curves just after 30 Å, as the polymers begin to push against and enter the bilayer.

After entry, the work done for HPT is much greater than that done for EHPT. EHPT shows a brief period of decreasing work just before 20 Å, indicating that the polymer begins to “slide down the potential” on entering. The HPT forward work curve does not show the same decrease. Although neither forward work curve can be considered to be an accurate estimate of the free energy of insertion, especially because these are single samples from two distributions, it is noteworthy that the total work to insert HPT (137 kcal/mol) is nearly 3 times that to insert EHPT (48 kcal/mol).

The work curves for the reverse pull show less of a difference between EHPT and HPT and more agreement in shape between the two polymer pulls. The work of EHPT removal from the bilayer is slightly higher than that of HPT removal (327 vs 291 kcal/mol), but this cannot conclusively be said to be due to differences between the two polymers; these values are close enough that the difference might reverse sign if both pulls were repeated. It should be noted that the work of removal was more than 100 kcal/mol higher for both polymers than the work of insertion. This leads to the reverse pull dominating the averaged curves of Figure 3. Taken at face value, the averaged work curves imply that the work of insertion for both polymers should be negative, with EHPT insertion being substantially more favorable than HPT insertion (145 vs 82 kcal/mol). However, as will be explained below, the reverse SMD pull appears to sample a nonphysical trajectory. Moreover, the presence of substantial frictional work may have led to local heating, altering the energetics of insertion and removal. Therefore, whereas the SMD work results may indicate the correct trend (because the forward pulls approximate a feasible path within the limits of frictional error), they cannot be considered to be a reliable quantitative estimate of the energy of insertion for either of the two model PATs.

The force curves for the forward and reverse EHPT and HPT pulls, as smoothed by a Gaussian window of 100 ps width, are shown in Figure 4. These curves corroborate the trend seen in the work results. HPT insertion forces are roughly equal to EHPT insertion forces until the polymers come into contact with the bilayer, at which point HPT forces increase and remain higher throughout most of the run. The HPT peak insertion force of 8 kcal/mol/Å is double the EHPT peak insertion force of 4 kcal/mol/Å. As with the work results, the reverse pull (removal) forces follow almost identical trajectories if the EHPT and HPT runs are overlaid, with the difference being that the EHPT force peaks slightly later (around 16 Å instead of 13 Å) and higher (18 vs 15 kcal/mol/Å) than the HPT force.

The insertion trajectories of EHPT and HPT reveal possible reaction paths and provide an explanation of the observed difference in the work curves. Selected frames from these trajectories are shown in Figure 5, and full trajectory movies are available as Supporting Information. Both polymers begin similarly, by “docking” with the membrane in a horizontal configuration that maximizes the contact between the hydrophobic side chains and the bilayer surface. From this configuration, the polymer breaches a hole in the polar head group layer and then inserts itself through this hole into the bilayer interior. During the course of these trajectories, the polymers adopt a relatively vertical configuration within the lipid phase, but this may be due to an insufficient relaxation time; different configurations were observed in the umbrella sampling runs reported below. The “sideways docking, interface destabilization, and bilayer insertion” path followed by these polymers is similar to the mechanism proposed for membrane-inserting peptides.⁴² The same path has also been observed in other simulations of transmembrane peptides^{8,9,11} and in a coarse-grained MD study of channel protein insertion.¹²

Supporting Information Available: The parameters used for this simulation are to be published elsewhere and are also available on request from the authors. Movies of the steered molecular dynamics insertion and removal trajectories for EHPT and HPT. This material is available free of charge via the Internet at <http://pubs.acs.org>. LA070214V

The difference in the insertion trajectories of EHPT and HPT lies in the way that they destabilize the head groups and insert. EHPT creates a hole that admits a single ring and then threads itself through in a ring-by-ring fashion, bending in the middle as it does so. This process is most clearly illustrated in the 3659 ps panel of the EHPT series in Figure 6. By contrast, HPT destabilizes the head group interactions at multiple points simultaneously and then inserts in a largely horizontal configuration, with multiple rings passing through the polar region at once. That process is visible from 3509 to 3970 ps in the HPT series of Figure 5 and Figure 6. These trajectories can explain the previously presented work and force curves. The EHPT work curve in Figure 3 remains relatively flat during the docking phase (roughly a 25–30 Å distance) and does not change slope until nearly 20 Å, when EHPT is breaching the head group layer. The HPT work curve, however, changes slope and begins to climb between 25 and 30 Å distance, demonstrating that HPT is already displacing bilayer molecules as it docks. The more disruptive nature of HPT's en bloc insertion also explains the continually high insertion forces seen in Figure 4.

When pulled from the center of the bilayer to the outside, EHPT and HPT show very similar work and force curves. Both polymers encounter the polar region (starting at the carbonyl oxygens) as a barrier, as evidenced by the upturn in the work curves around 5–10 Å. The trajectories are also similar, and two key frames from the EHPT trajectory are shown in Figure 7. Both EHPT and HPT make a hole in the head groups and exit in a stretched vertical configuration. Unlike the forward SMD pull, no peak is seen on either work curve corresponding to this hole formation. It may be that this peak exists but is overwhelmed by the work required to continue dragging the polymer out of the membrane. Both polymers also experience large forces resisting their exit. They are continually in an extended conformation, implying that the entire polymer chain is experiencing tension and stretching. The reason for this high tension is seen in the frames of Figure 7. The DMPC tails bind strongly (presumably through van der Waals attractions) to the side chains of EHPT and HPT, with the attraction being so strong that one tail is temporarily “dragged” into the aqueous phase once the polymer has exited. The explanation for the high forces and resulting high work for both removal pulls is thus revealed: a continual forming and breaking of nonbonded attractions as the polymer moves out of the lipid phase.

Dragging of lipids alongside a hydrophobic molecule has also been observed in SMD studies of the removal of a monotopic protein from a bilayer¹⁰ but was not seen in a study of lipids being directly pulled out of a DPPC bilayer.⁴³ Dragging is therefore not an obligate feature of SMD pulls in a membrane environment and may be a sign of an overly rapid pull. More importantly, the lipid dragging combined with other features of the reverse SMD pulls suggests that these runs sampled a nonphysical trajectory. As noted above, both reverse pulls showed substantial deviation between commanded and actual polymer-center-to-bilayer-center distances, calling into question the applicability of the stiff-spring assumption. APAT in an aqueous medium should attempt to self-aggregate to reduce the exposed surface area, but the polymers in these reverse SMD runs show an extended conformation until they break free of their attached lipid tails. Moreover, the energy of removing a lipid from a DMPC membrane is so high (20 kcal/mol) that removal is not likely to occur in a physical trajectory.⁴⁴ In short, it appears that the reverse SMD is overly dominated by frictional forces and that multiple slower pulls in both directions would be necessary to recover the PMF effectively for polymer insertion. However, the forward runs were likely slow enough to capture an approximation of one reasonable path in each case. Although they are not the only possible paths, these trajectories can be used to obtain umbrella sampling and a PMF with less overall computational effort.

Umbrella Sampling Energy Estimation

The PMFs for EHPT and HPT insertion into the DMPC bilayer, as computed from umbrella sampling, are shown in Figure 8. By comparing these to the SMD results in Figure 3, one sees that the SMD curves predict the correct trend but miss key features. Both polymers show relatively flat potentials in the water region, which extends to an approximately 30 Å center-to-center distance. At that point, both polymers show an energy barrier, with HPT facing a taller (1.53 kcal/mol higher than for EHPT) but narrower barrier. Past the barrier, the potentials become quite different. EHPT descends a slope that ends at 9–10 Å, leaving a flat potential within the lipid portion of the bilayer. HPT, conversely, shows a deeper well at 12 Å. At first glance, the PMF curves seem to imply that HPT insertion is even more favorable than EHPT insertion, at –16 kcal/mol compared to EHPT’s minimum of –10 kcal/mol. However, this is a false impression because true insertion into the lipid phase begins only 10 to 12 Å from the bilayer center. HPT’s PMF minimum occurs at a center-to-center distance of 12 Å, a point before true insertion. EHPT has no such minimum and is able to travel fully into the lipid phase, reaching –6 kcal/mol at 0 Å compared to EHPT’s –10 kcal/mol.

To illustrate further the configurations corresponding to these energy minima, representative frames at selected distances are shown in Figure 9 and Figure 10. At 30 Å, as both polymers are docking with the membrane, a difference can already be seen: HPT is beginning to insert its head into the polar layers of the membrane whereas EHPT is seeking to maximize its area of contact with the membrane. At their respective PMF maxima, both polymers are seen to be starting their insertions, following the different modalities seen in the forward SMD trajectories. The reason for these two different insertion techniques becomes more clear when the conformations at 12 Å are considered. EHPT has created a hole and is threading itself through. Meanwhile, HPT has already sunk to its optimal resting place, at approximately the level of the carbonyl oxygens. This is also the deepest level to which water penetrates so that HPT lies at the boundary between polar and nonpolar solvent phases.⁴⁵ The en bloc horizontal insertion observed in the forward SMD pull makes sense in this context: if HPT’s optimal state is one of an admixture with the head groups and glycerol backbones of DMPC, then during the SMD run, it will pass through that configuration when directed to the proper Z coordinate. The applied SMD force will cause HPT to sink further past the optimal point at 12 Å, but it will prefer to retain its horizontal configuration rather than reorienting to a more vertical, EHPT-like configuration.

It is equally informative to consider the configurations of both polymers at 6 Å (sinking through the lipid phase) and 0 Å (the bilayer center), both of which are shown in Figure 10. At 6 Å, EHPT is effectively completely inserted and can be seen “reaching out to the next leaflet”. HPT, by contrast, is in a twisted conformation that appears to attempt to minimize its contact with the lipid tails. At 0 Å, EHPT forms an electrical bridge between the two membrane leaflets. HPT at 0 Å is in a planar extended conformation in the low-density space between leaflets and is not close enough to either DMPC/water interface to form an effective bridge.

Taken together, these features of the PMF and the associated polymer configurations highlight two key differences between EHPT and HPT. First, it is not energetically favorable for HPT to insert fully into the membrane. The minimum point of the HPT insertion PMF is at 12 Å, and the polymer is likely to become “stuck” at this point. This prevents HPT from entering the hydrocarbon layer, whereas the free-energy landscape for EHPT permits free movement within all regions of the bilayer. Second, if HPT does escape the well at 12 Å and move to the bilayer center, then it will be forced into the horizontal orientation seen in the 0 Å panel of Figure 10. This configuration does not span the membrane and thus seems unlikely to conduct current across it effectively. EHPT, by contrast, is seen to adopt a bilayer-spanning conformation.

Discussion

The results presented above can explain our prior BLM observations⁴ in terms of the energetics of PAT insertion into a model lipid bilayer. The SMD pulls suggest that the insertion of EHPT and HPT follows two different paths, with the path for HPT being less energetically favorable. Although SMD was not able to provide a good estimate of the actual energy of insertion because of the reverse pulls being dominated by the irreversible work, the umbrella sampling runs were used in this estimate as a seed to extract an accurate PMF. The longer per-window simulation time during umbrella sampling also allows the polymer to relax to its near-optimum configuration at each point. It should be noted that we cannot absolutely guarantee that the observed configurations are the global minima for EHPT and HPT because the relaxation time of this system is not known. We believe that the 3 ns used for each umbrella sampling window is sufficient, but even longer simulations (possibly using alternate starting points for each window) could find alternate minima. Therefore, the results that were observed in these simulations suggest two explanations for our prior empirical observation that HPT is unable to increase a BLM's conductance even though EHPT does:

1. Because HPT's PMF minimum is far from the bilayer center and relatively close to the bilayer surface, HPT becomes stuck at the glycerol/carbonyl level with its long axis perpendicular to the bilayer normal. It never comes close to crossing the bilayer and thus cannot electrically bridge it.
2. (2) HPT does reach the bilayer center and is highly conductive in this medium, but as seen in Figure 9, it is again locked into a configuration with its long axis perpendicular to the membrane normal. In this configuration, it is too isolated from the potentials on either side of the bilayer to conduct current effectively.

Because the two explanations are not mutually exclusive, the true situation *in vitro* most likely involves both phenomena occurring in parallel. However, the first explanation (failure of HPT to breach the bilayer fully) should dominate, if only because it corresponds to HPT being in its lowest-energy conformation. It should be noted that the relatively similar energy barriers (3.26 kcal/mol for EHPT vs 4.79 kcal/mol for HPT) required to breach the polar head groups have no bearing on the relative insertability of the two polymers because the final inserted or noninserted configuration depends entirely on the location of the PMF minimum.

The deeper question not yet answered by these simulations is *why* EHPT is able to dissolve well in the lipid phase of the DMPC membrane and adopt the bridging conformations observed in these simulations. The answer almost certainly involves the branched 2-ethylhexyl side chain, which is the only chemical difference between EHPT and HPT. However, there are many mechanisms through which side-chain branching could have an effect. One is through simple steric hindrance and the resultant disorder of the system. EHPT's branched side chain may simply be more able to disrupt the packing of neighboring molecules, allowing the polymer to maneuver itself between them. It is known that PATs whose side chains do not pack well are not able to form 3D-ordered materials.⁴⁶ Branching also permits an interesting configuration in which the branches rotate so that the polymer backbone is entirely wrapped in a "solvation shell" of alkanes; this conformation is not available with straight side chains. Long-chain alkanes such as the tails of a bilayer are believed to be good solvents for PAT side chains but poor solvents for backbone thiophenes, and branched side chains may effectively "shield" the backbone from the solvent. If shielding is the key, then side chains with longer branches should be even more effective. Because branched-side-chain PATs (and polythiophenes with bulky side chains in general) are nontrivial to synthesize, further *in silico* testing of these hypotheses would be desirable. One might proceed by repeating the simulations in this article with a variety of branched side chains (e.g., different branch lengths, different

branch points, and a larger number of branches) and with longer or shorter straight alkyl side chains.

Aggregation phenomena must also be considered when comparing these results to prior empirical studies. It is well known that regioregular PATs readily aggregate, even in dilute solution.⁴⁷⁻⁴⁸ The solutions used in the BLM work were highly concentrated and therefore almost certainly contained a substantial fraction of aggregates. This suggests that what would be inserted into the membrane in a real device is not a single PAT molecule but an aggregate containing multiple chains. The flexibility of such an aggregate could be quite different from that of the single molecule, and there is evidence that more flexible PATs will have more flexible aggregates.¹⁷ Because EHPT is not solvatochromic (i.e., it retains its random-chain behavior even in poor solvent), its aggregates may remain relatively flexible and disordered and thus able to insert. HPT aggregates should be stiff and rodlike and may not be able to insert. It would therefore be highly valuable to perform follow-up MD simulations using aggregates instead of single chains. A principal barrier to such studies is the lack of knowledge regarding the correct structure of PAT aggregates. A set of candidate aggregate structures must first be generated through a mechanism such as replica exchange simulation in implicit solvents.

In conclusion, the results of the MD simulations carried out in this article have shed light on mechanisms that can explain our previous results and argue for the feasibility of the transmembrane PAT electrode concept diagrammed in Figure 1. They have also demonstrated the utility of our new PAT force field parameters for modeling the behavior of PATs for any number of applications. In the process, new questions have been raised regarding the optimal PAT structure for our proposed device, and these questions can in turn be answered by future *in silico*, *in vitro*, and eventually *in vivo* experiments. We are continuing forward with answering these questions and further developing this electrode technology, and we believe that it will become a valuable tool for the biosensing community once it is fully validated.

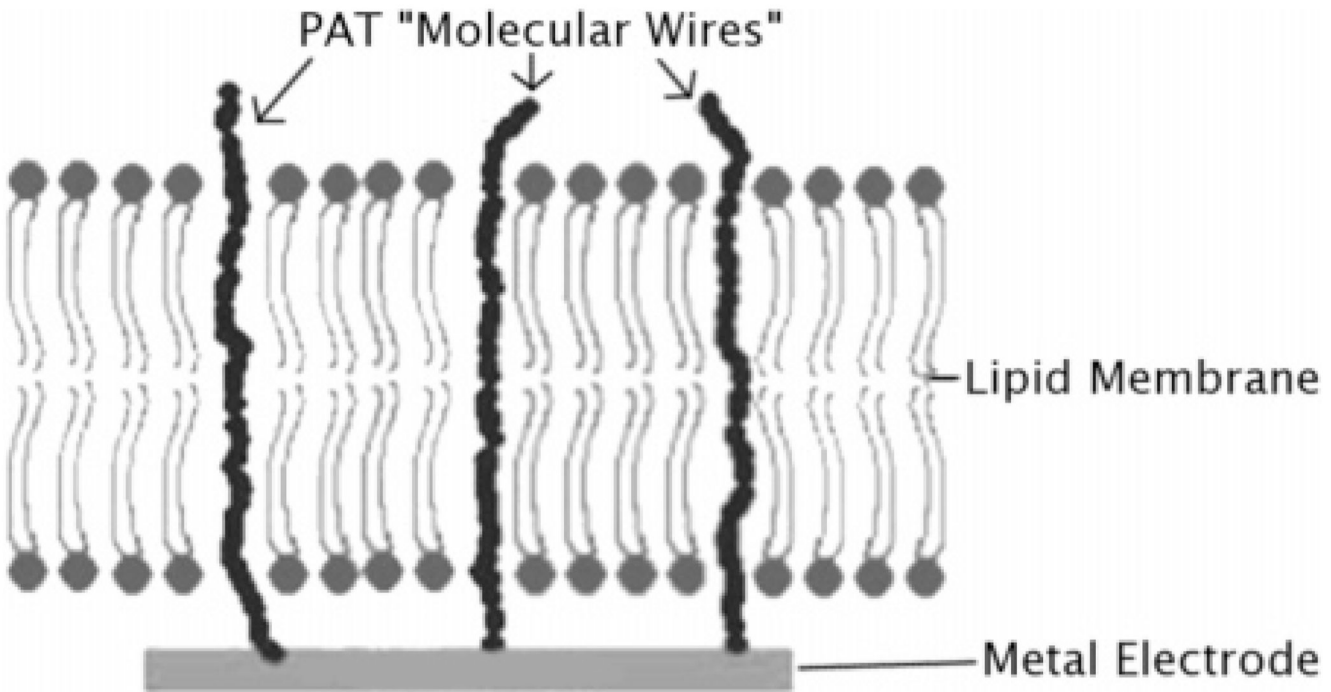
Acknowledgments

A.S.W. was funded during this research by a Ruth L. Kirchstein National Research Service Award (grant number F30 NS051866-01) from the National Institutes of Health. The simulations reported here were carried out using the Terascale Computing System and Cray XT3 machines of the Pittsburgh Supercomputing Center, and we thank PSC for its generous grants of computer time to M.K. (NSF PACI CHE030007P) and Y.M. M.K.'s research is also supported by the NIH (GM067962-01).

References

1. Mabeck JT, Malliaras GG. *Anal. Bioanal. Chem.* 2006;384:343–353. [PubMed: 16079978]
2. Barbarella G, Melucci M, Sotgiu G. *Adv. Mater.* 2005;17:1581–1593.
3. Widge AS, Jeffries-El M, Cui X, Lagenaar CF, Matsuoka Y. *Biosens. Bioelectron.* 2007;22:1723–1732. [PubMed: 17015008]
4. Widge AS, Matsuoka Y. *Proc. 26th Ann. Intl. Conf. IEEE EMBS* 2004:4330–4333.
5. Bachar M, Becker OM. *Biophys. J.* 2000;78:1359–1375. [PubMed: 10692322]
6. Lin J, Baumgaertner A. *Biophys. J.* 2000;78:1714–1724. [PubMed: 10733954]
7. Kandasamy SK, Larson RG. *Chem. Phys. Lipids* 2004;132:113–132. [PubMed: 15530453]
8. Tieleman DP, Berendsen HJC, Sansom MSP. *Biophys. J.* 2001;80:331–346. [PubMed: 11159406]
9. Nymeyer H, Woolf TB, Garcia AE. *Proteins: Struct., Funct., Bioinf.* 2005;59:783–790.
10. Fowler PW, Coveney PV. *Biophys. J.* 2006;91:401–410. [PubMed: 16632499]
11. Bond PJ, Sansom MSP. *J. Am. Chem. Soc.* 2006;128:2697–2704. [PubMed: 16492056]
12. Lopez CF, Nielsen SO, Ensing B, Moore PB, Klein ML. *Biophys. J.* 2005;88:3083–3094. [PubMed: 15722425]

13. Vemparala S, Saiz L, Eckenhoff RG, Klein ML. *Biophys. J* 2006;91:2815–2825. [PubMed: 16877515]
14. Contera SA, Lemaitre V, de Planque MRR, Watts A, Ryan JF. *Biophys. J* 2005;89:3129–3140. [PubMed: 16085762]
15. Shibaev P, Arzhakov M, Schaumburg K, Vinokur R, Bjornholm T, Greve D, Komolov A, Norgaard K. *J. Polym. Sci., Part B: Polym. Phys* 1999;37:2909–2917.
16. Shibaev P, Schaumburg K. *Synth. Met* 2001;124:291–294.
17. Shibaev P, Schaumburg K, Bjornholm T, Norgaard K. *Synth. Met* 1998;97:97–104.
18. Xie H, O'Dwyer S, Corish J, Morton-Blake D. *Synth. Met* 2001;122:287–296.
19. O'Dwyer S, Xie H, Corish J, Morton-Blake D. *J. Phys: Condens. Matter* 2001;13:2395–2410.
20. Morton-Blake D, Yurtsever E. *J. Mol. Liq* 2006;124:106–113.
21. Leith D, Morton-Blake D. *Mol. Simul* 2005;31:987–997.
22. Cirak J, Tomcik P, Barancok D, Bolognesi A, Ragazzi M. *Thin Solid Films* 2002;402:190–194.
23. Pal S, Milano G, Roccatano D. *J. Phys. Chem. B* 2006;110:26170–26179. [PubMed: 17181272]
24. Lindahl E, Hess B, van der Spoel D. *J. Mol. Model* 2001;7:306–317.
25. De Groot BL, Tieleman DP, Pohl P, Grubmuller H. *Biophys. J* 2002;82:2934–2942. [PubMed: 12023216]
26. Case DA, Cheatham TE III, Darden T, Gohlke H, Luo R, Merz KM Jr, Onufriev A, Simmerling C, Wang B, Woods R. *J. Computat. Chem* 2005;26:1668–1688.
27. Takaoka Y, Pasenkiewicz-Gierula M, Miyagawa H, Kitamura K, Tamura Y, Kusumi A. *Biophys. J* 2000;79:3118–3138. [PubMed: 11106617]
28. Widge AS. Ph.D. Thesis. Carnegie Mellon University; 2007 Jan. Available as CMU-RI-TR-07-03
29. Widge AS, Matsuoka Y, Kurnikova M. *J. Comput. Chem*. submitted for publication.
30. Humphrey W, Dalke A, Schulten K. *J. Mol. Graphics* 1996;14:33–38.
31. Petrache HA, Dodd SW, Brown MF. *Biophys. J* 2000;79:3172–3192. [PubMed: 11106622]
32. Anézo C, de Vries AH, Höltje H-D, Tieleman DP, Marrink S-J. *J. Phys. Chem. B* 2003;107:9424–9433.
33. Phillips JC, Braun R, Wang W, Gumbart J, Tajkhorshid E, Villa E, Chipot C, Skeel RD, Kale L, Schulten K. *J. Comput. Chem* 2005;26:1781–1802. [PubMed: 16222654]
34. Balsera M, Stepaniants S, Izrailev S, Oono Y, Schulten K. *Biophys. J* 1997;73:1281–1287. [PubMed: 9284296]
35. Park S, Schulten K. *J. Chem. Phys* 2003;120:5946–5961. [PubMed: 15267476]
36. Gumbart J, Schulten K. *Biophys. J* 2006;90:2356–2367. [PubMed: 16415058]
37. Stepaniants S, Izrailev S, Schulten K. *J. Mol. Model* 1997;3:473–475.
38. Kosztin I, Barz B, Janosi L. *J. Chem. Phys* 2006;124:064106.
39. Park S, Khalili-Araghi F, Tajkhorsid E, Schulten K. *J. Chem. Phys* 2003;119:3559–3566.
40. Chodera JD, Swope WC, Pitera JW, Seok C, Dill KA. *J. Chem. Theory Comput* 2007;3:26–41.
41. Kumar S, Bouzida D, Swendsen RH, Kollman PA, Rosenberg JM. *J. Comput. Chem* 1992;13:1011–1021.
42. Shai Y. *Biochim. Biophys. Acta* 1999;1462:55–70. [PubMed: 10590302]
43. Marrink S, Berger O, Tieleman DP, Jahnig F. *Biophys. J* 1998;74:931–943. [PubMed: 9533704]
44. Tieleman DP, Marrink S-J. *J. Am. Chem. Soc* 2006;128:12462–12467. [PubMed: 16984196]
45. Tieleman DP, Marrink SJ, Berendsen HJC. *Biochim. Biophys. Acta* 1997;1331:235–270. [PubMed: 9512654]
46. Prosa TJ, Winokur MJ, Moulton J, Smith P, Heeger AJ. *Macromolecules* 1992;25:4364–4372.
47. Heffner GW, Pearson DS, Gettinger CL. *Polym. Eng. Sci* 1995;35:860–867.
48. Yue S, Berry GC, McCullough RD. *Macromolecules* 1996;29:933–939.

**Figure 1.**

Schematic of the proposed “molecular wire” electrode mechanism. PATs, tethered in a SAM to a metal electrode, penetrate a lipid bilayer membrane (either as single chains or linear aggregates) and are able to access intracellular electrical signals. The success of the mechanism depends on proper tailoring of the PAT side chains to achieve lipid solubility.

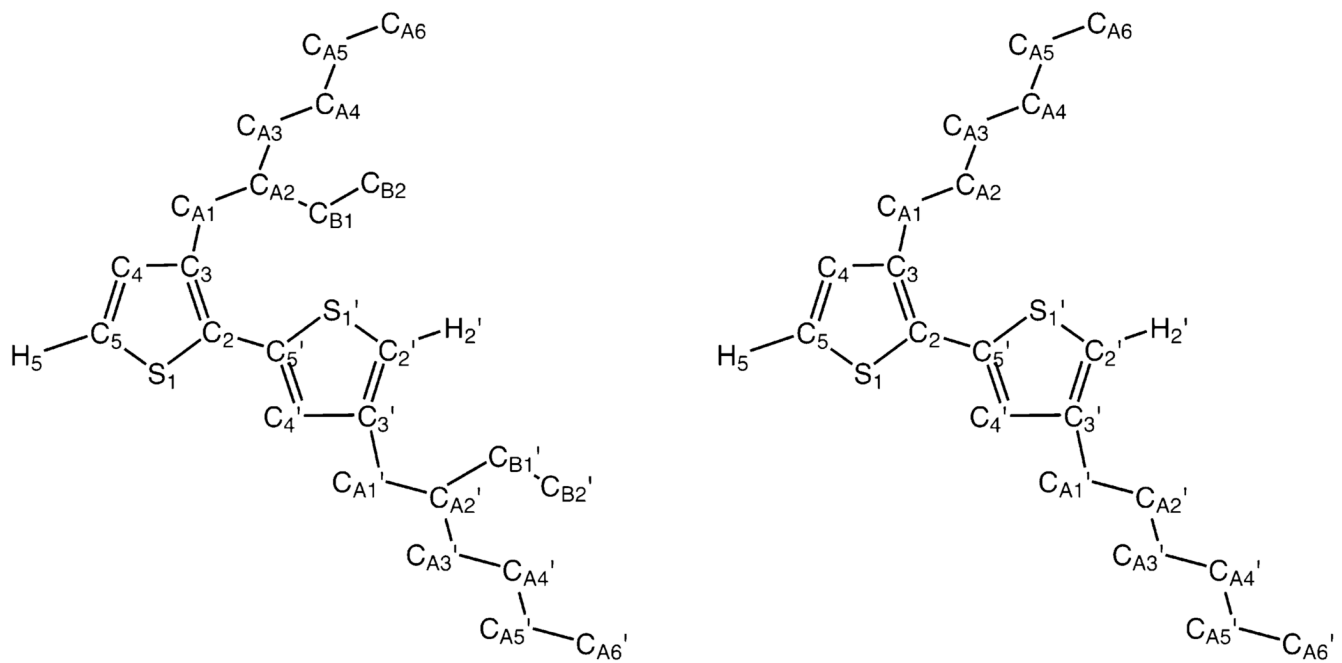
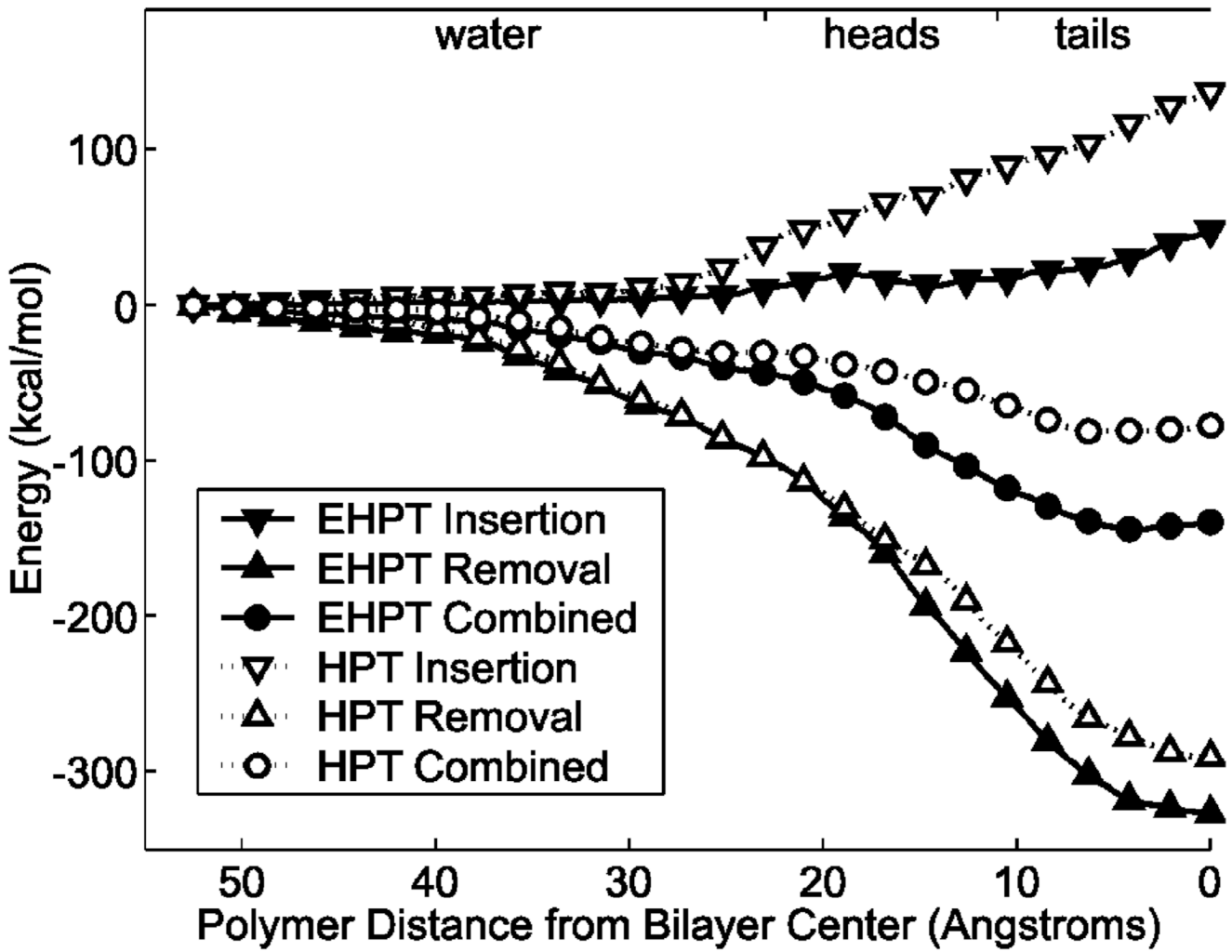
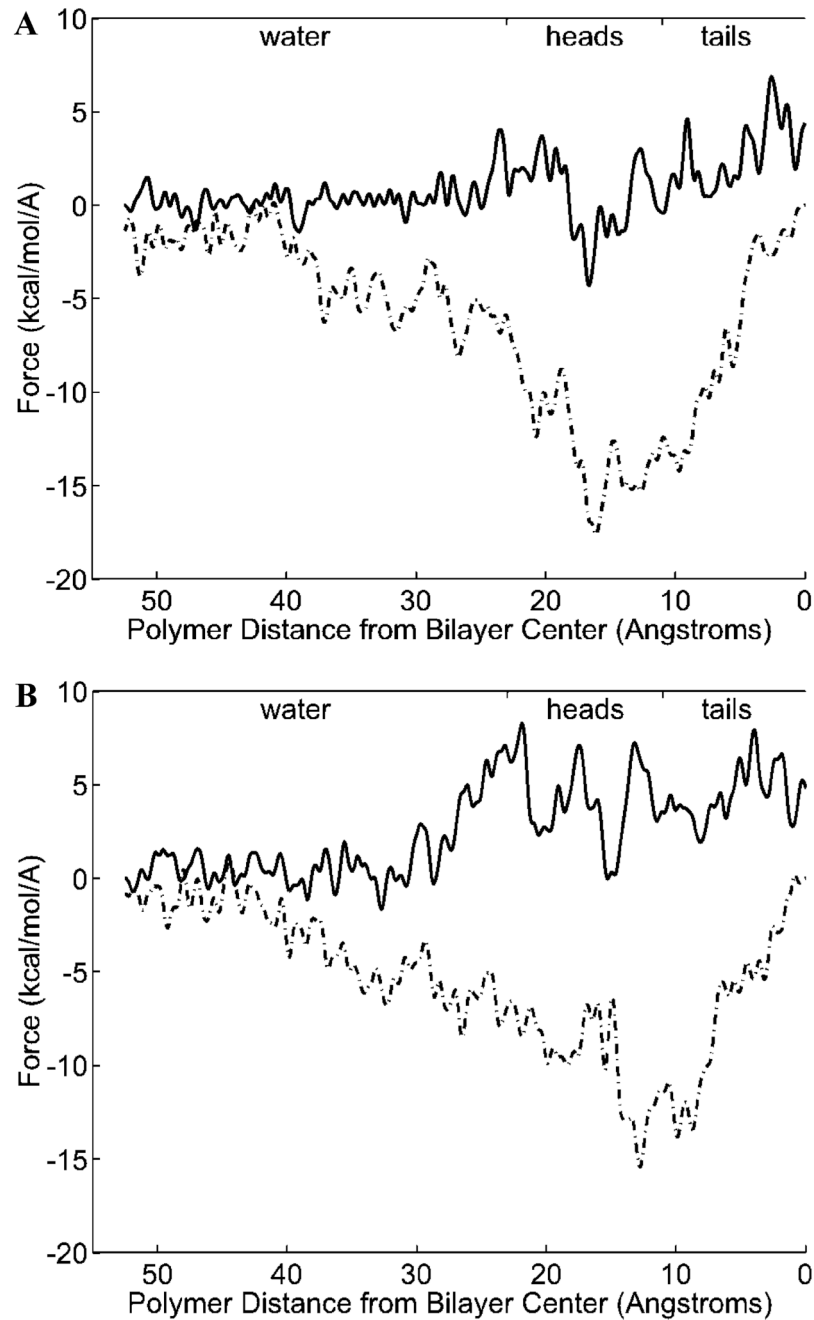


Figure 2.

Structure of ethylhexyl (EHPT, left) and hexyl (HPT, right) dimers, with side-chain hydrogens removed for clarity. EHPT bears a branched alkyl side chain, but HPT's is straight. The difference in side chains leads to different solubility in common solvents, which in turn explains the results of the current investigation.

**Figure 3.**

Forward (downward arrows), reverse (upward arrows), and averaged (circles) work curves for the steered molecular dynamics pulling of EHPT (solid lines and markers) and HPT (dotted lines with open markers) into and out of the lipid bilayer. HPT requires substantially more work than EHPT for insertion (137 vs 48 kcal/ mol). HPT also requires less work for removal, although the difference is not as large as for insertion (291 vs 327 kcal/mol). The averaged curves are dominated by the influence of the nonphysical reverse pulls but suggest that EHPT insertion is more energetically favorable than HPT insertion.

**Figure 4.**

Force curves for steered molecular dynamics pulling of EHPT (A) and HPT (B) into and out of the lipid bilayer, smoothed with a 100 ps Gaussian window. The forward pull forces are shown as a solid line, and reverse pull forces are shown as a dotted-dashed line. Forces are equal in the water phase, but HPT requires higher forces to achieve initial bilayer entry (8 kcal/mol/Å peak vs 4 kcal/mol/Å peak for EHPT). The HPT force curve remains above the EHPT force curve for most of the forward pull through the lipid phase. Forces on the reverse pull are better matched, but EHPT has a slightly higher peak force as it begins to leave the bilayer (18 vs 15 kcal/mol/Å for HPT). The removal forces for both polymers are substantially higher than the insertion forces.

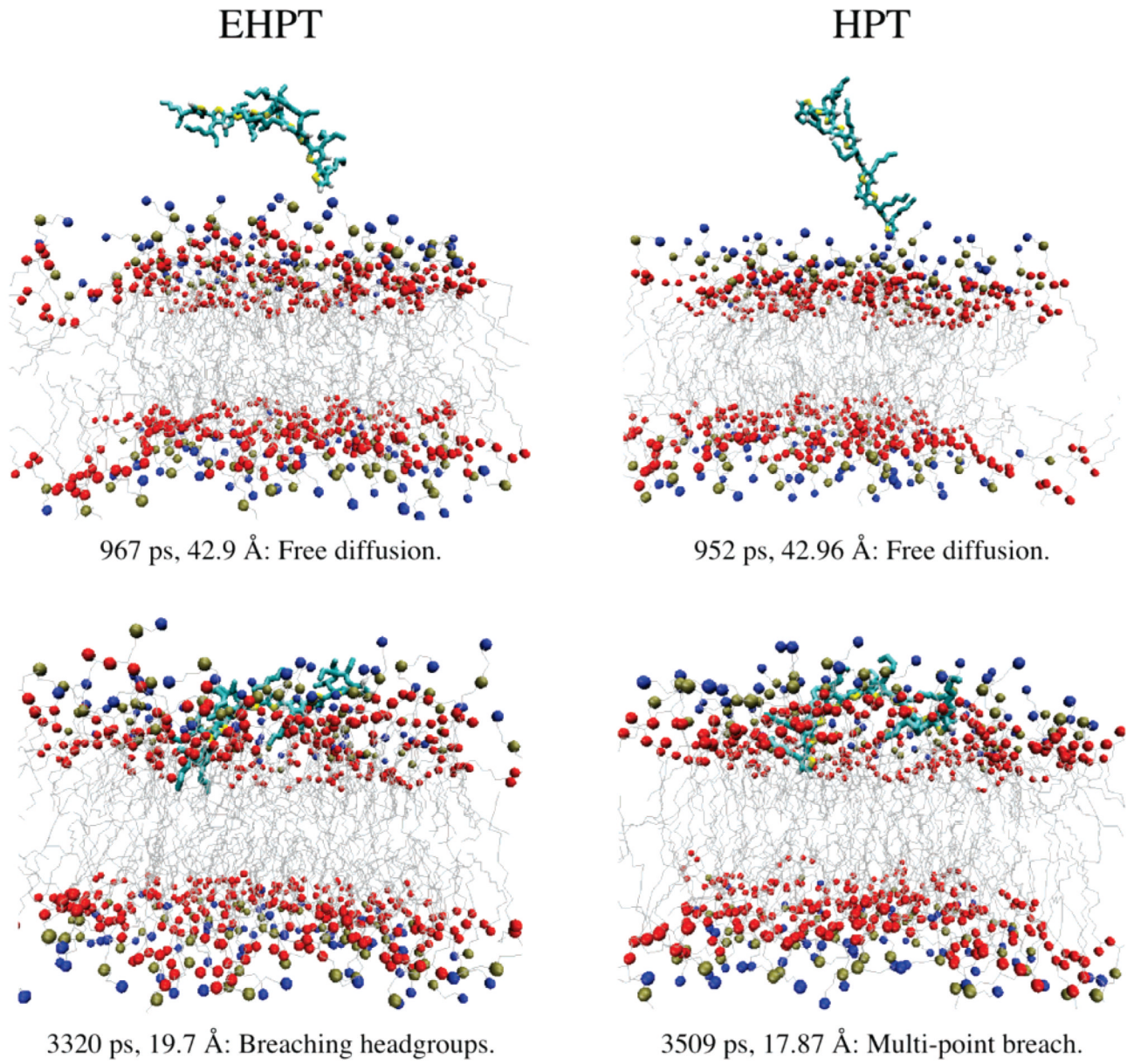


Figure 5.

Selected frames from the SMD insertion trajectories of EHPT and HPT showing the approach to the membrane and the breach of the polar layer. Blue, tan, and red spheres represent choline, phosphate, and oxygen, respectively. HPT shows a more disruptive insertion pathway involving a larger “hole” in the head group plane.

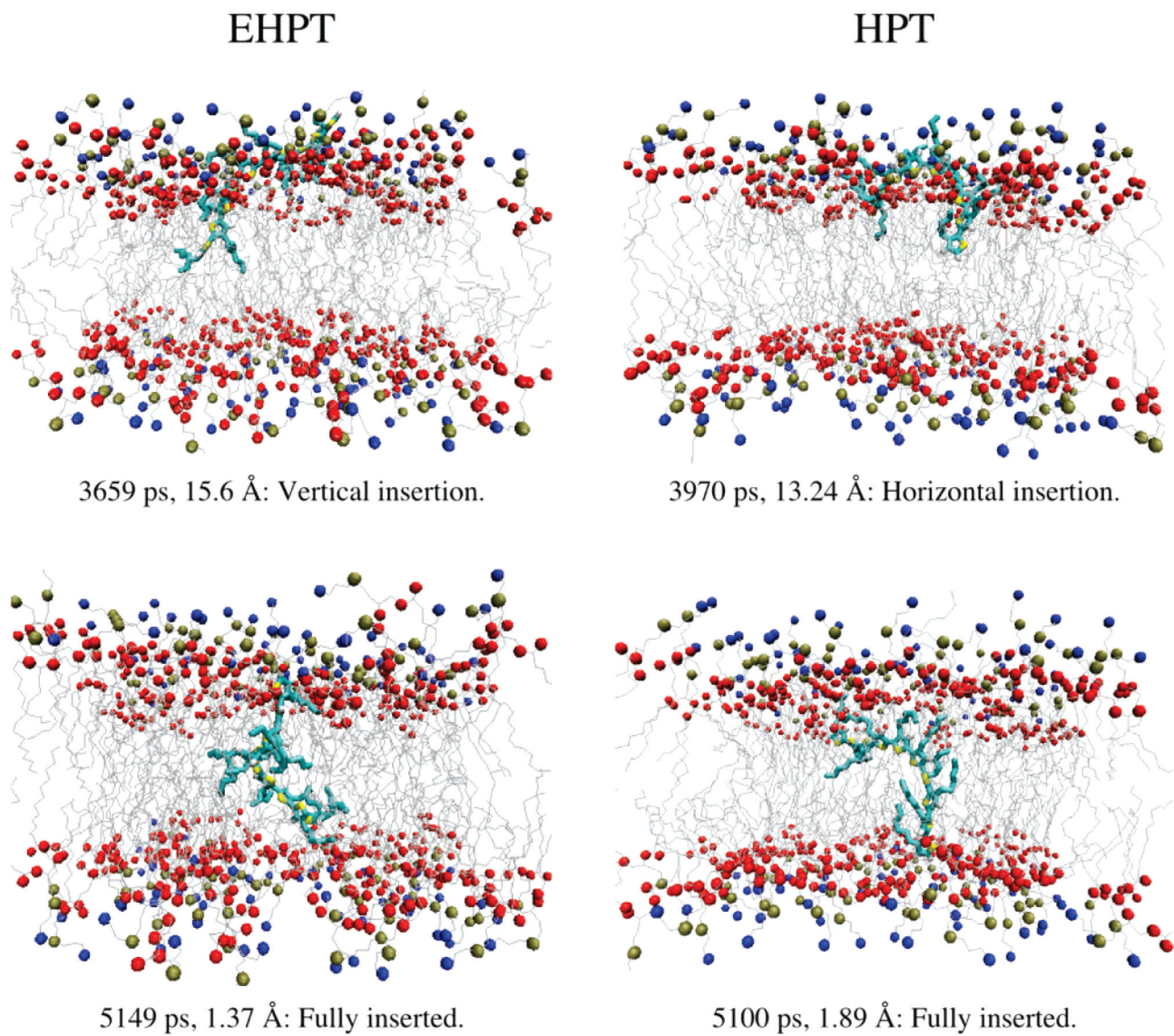
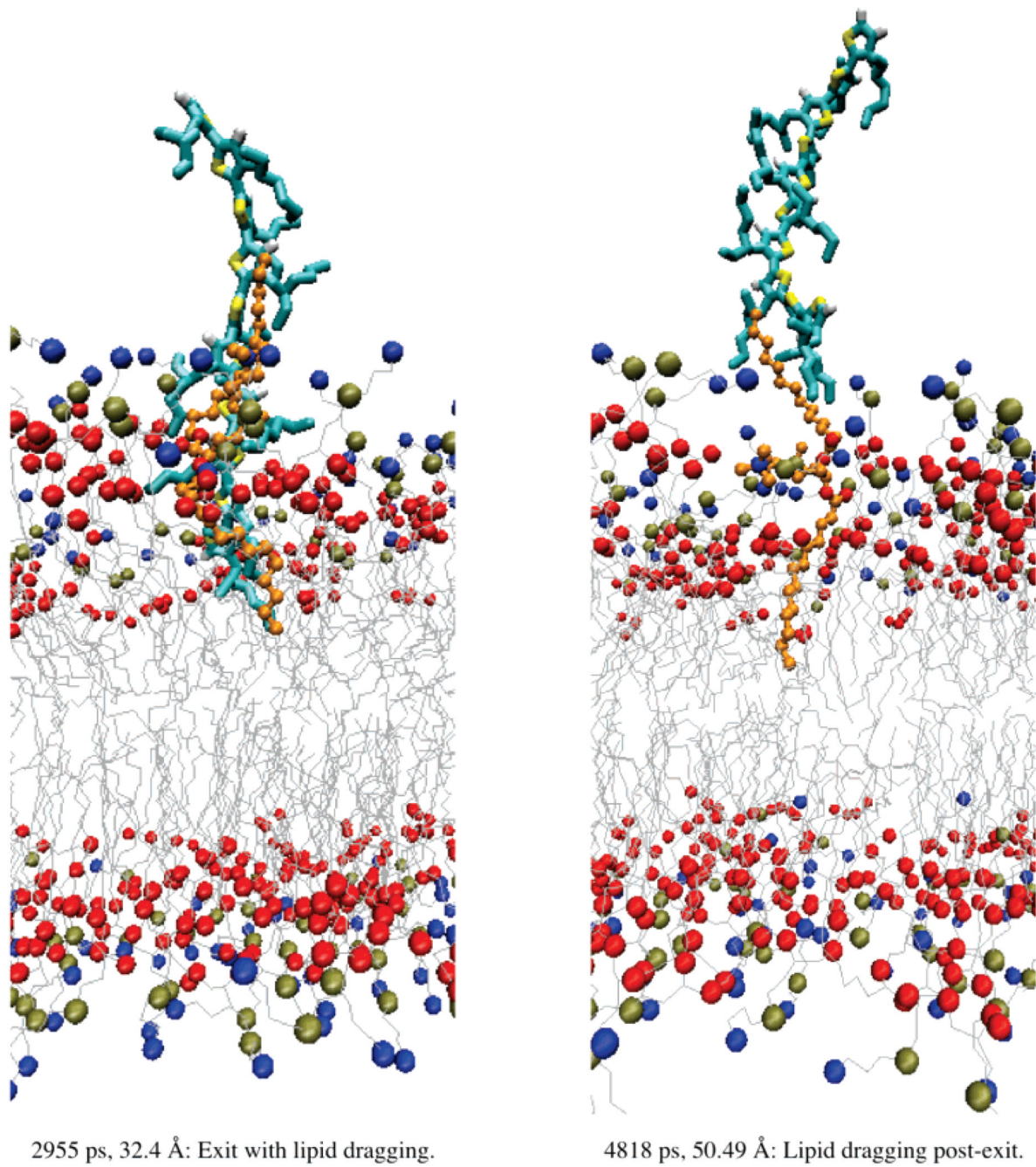


Figure 6.

Additional frames from the EHPT and HPT SMD insertion trajectories showing the insertion of the polymers and their final configurations within the hydrocarbon phase of the bilayer. The colors are the same as in Figure 5. Both polymers show similar final configurations under SMD, but HPT insertion involves more disruption of the membrane structure, as seen in the upper-right panel.

**Figure 7.**

Selected frames from the EHPT SMD removal trajectory. The colors are the same as in Figure 5, with additional highlighting of one DMPC lipid in the upper leaflet (orange). As the polymer is forced out of the bilayer, it adopts an extended conformation because of substantial tensile forces. As the polymer exits, it “drags” the alkyl tail of one lipid with it, even after the polymer has fully exited.

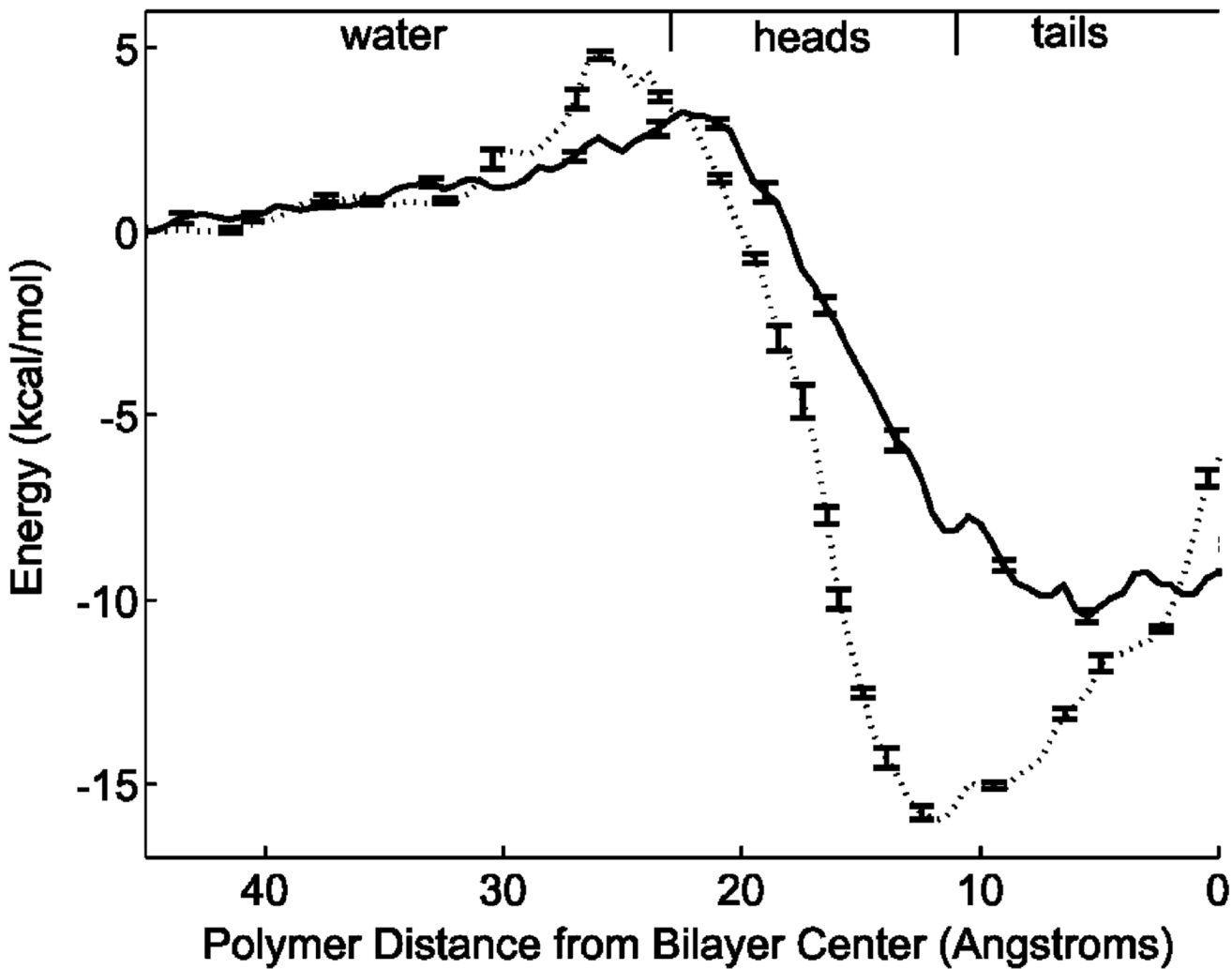


Figure 8.

Potential of mean force for EHPT (solid line) and HPT (dotted line) insertion into the lipid bilayer, as calculated from 28-window umbrella sampling. The potentials remain somewhat rugged because of the limited amount of sampling. However, as can be seen from the small size of the error bars, they are qualitatively correct. EHPT shows a steep descent to a broad, flat-bottomed well within the bilayer, suggesting that it should be able to diffuse freely within the lipid phase. HPT has an even steeper descent but is not free to diffuse. The HPT PMF shows a deep well around 12 Å, where HPT is likely to become trapped without fully inserting.

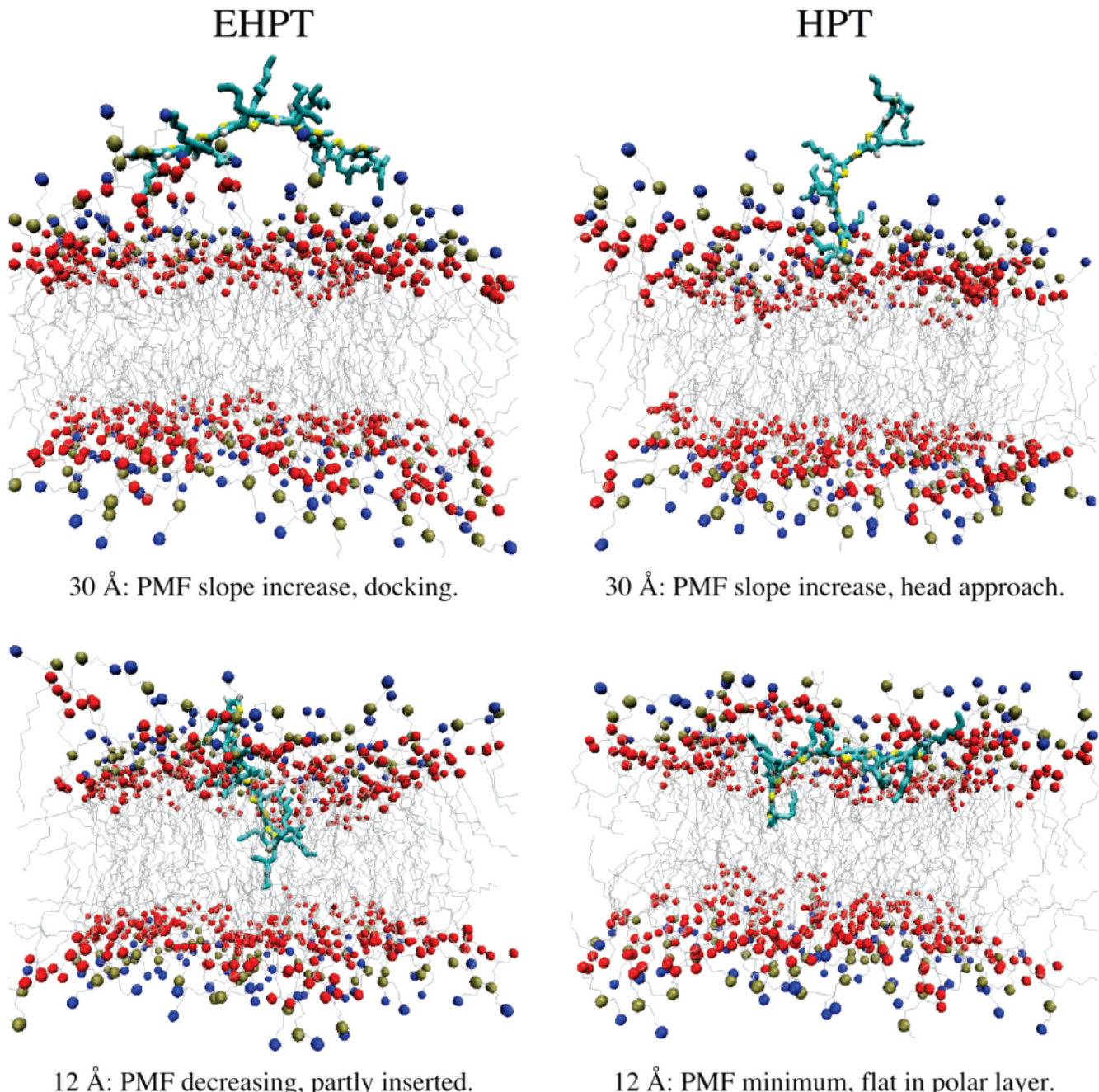


Figure 9.

Selected umbrella sampling configurations for EHPT and HPT. The colors are the same as in Figure 5. Both polymers adopt similar configurations at the PMF peak, but their insertion behaviors diverge by 12 Å. HPT has reached its PMF minimum and adopted a horizontal conformation, and EHPT is just beginning to insert.

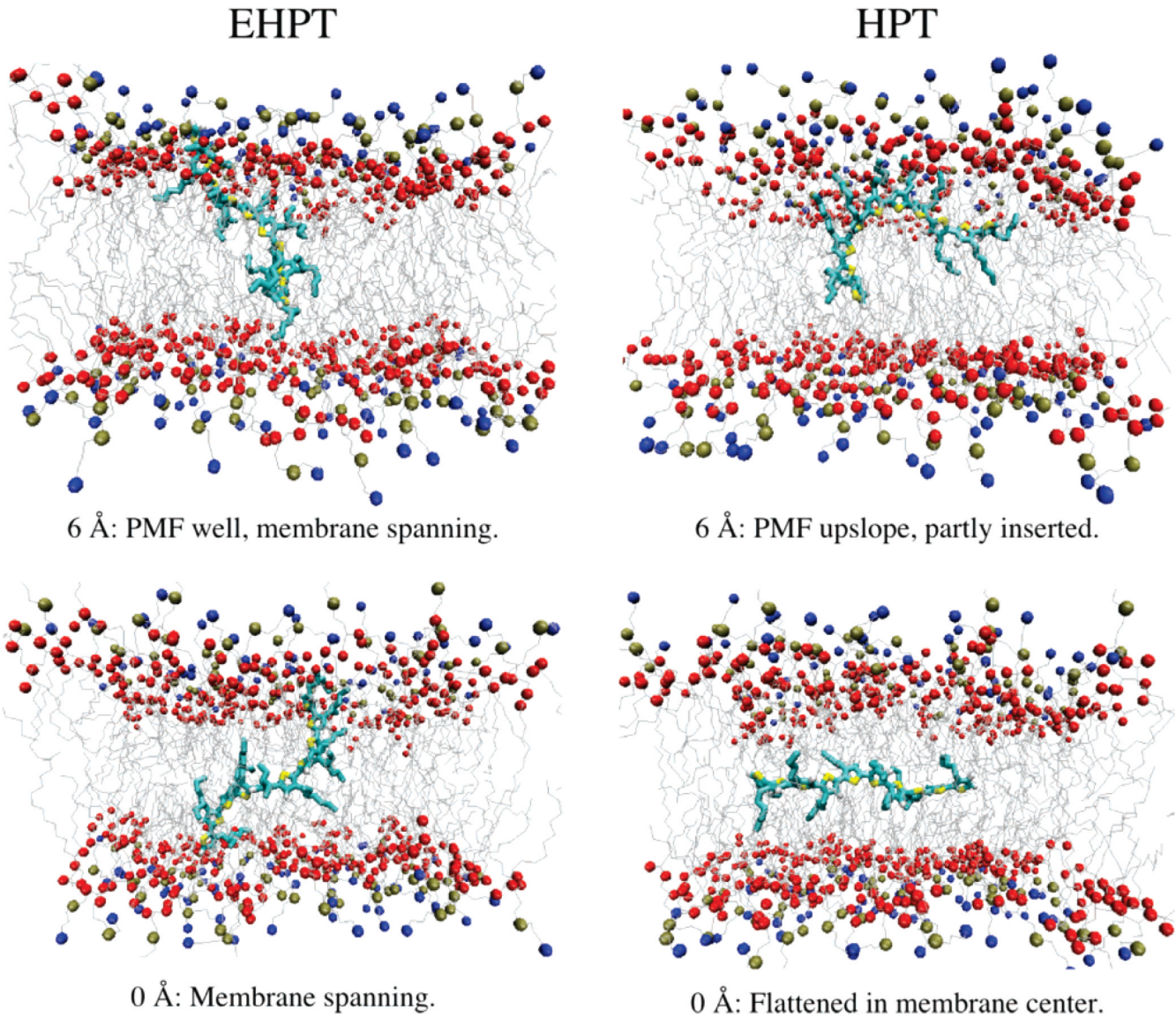


Figure 10.

Additional conformations from umbrella sampling. The colors are the same as in Figure 5. As EHPT moves deeper into the bilayer, it effectively spans the membrane and creates an electrical bridge. As HPT moves deeper (and climbs back up the far energy slope of its PMF), it remains in a horizontal conformation and is unable to span the membrane.